Axial Thiophene–Boron(subphthalocyanine) Dyads and Their Application in Organic Photovoltaics

Clayton E. Mauldin,[†,‡] Claudia Piliego,[†,‡] Daniel Poulsen,[†,‡] David A. Unruh,[†,‡] Claire Woo,[†,‡] Biwu Ma,[*,‡] Justin L. Mynar,[†] and Jean M. J. Fréchet[*,†,‡]

College of Chemistry, University of California, Berkeley, California 94720, and Materials Sciences Division, Lawrence Berkeley National Laboratory, Berkeley, California 94720

ABSTRACT We report the synthesis and characterization of boron(subphthalocyanine) derivatives with bithiophene and quaterthiophene as axial ligands, i.e., thiophene–subphthalocyanine dyads (nT-SubPcs), and their application in organic photovoltaic cells (OPVs). Thin films of nT-SubPcs prepared via solution processing can act as the electron donor in bilayer OPVs with evaporated C_{60} as the electron acceptor. The photophyscial and morphological properties of the nT-SubPcs are studied to rationalize OPV device parameters. The single-crystal X-ray structure is solved for two dyads to show the molecular structures in the solid state, and UV–vis spectroscopy and fluorescence spectroscopy are used to characterize the effect of conjugated thiophene ligands on the photophysical properties, i.e., absorption and photoluminescence quantum yield. Cyclic voltammetry, density functional theory (DFT) calculations, and low-temperature photoluminescence spectra show that photoluminescence yields depend on the overall flexibility of the SubPc derivatives and not on the oxidation potential or electronic relationship of the ligand and macrocycle molecular orbitals. We show with grazing-incidence X-ray scattering and atomic force microscopy (AFM) that careful choice of ligand structure can improve the crystallinity of thin films that leads to a relative increase in short-circuit current in OPV device. Our work clearly demonstrates that SubPcs can be used as light-harvesting chromophores in a matrix of a crystalline organic semiconductor for OPVs.

KEYWORDS: boron(subphthalocyanine) • organic photovoltaic • oligothiophene • semiconductor • photoluminescence

INTRODUCTION

The use of solution-processable small molecules as components for organic solar cells is attractive because of the desirable intrinsic properties of these materials: high molecular purity, reproducible and scalable synthesis, tunable structural and electronic properties, high light absorbency with controllable sensitivity in the low-red and infrared regions, and ease of processing in device fabrication. As new materials are developed and device processing techniques are enhanced, the power conversion efficiencies (PCEs) of small molecule solar cells have steadily improved over a short period of time (1–3) involving a range of compounds from polyacenes to phthalocyanines and many other organic dyes (4, 5).

One class of small molecule materials of great interest to us is boron subphthalocyanine (SubPc) and its derivatives. A SubPc has a nonplanar pyramid-shaped structure, wherein the boron atom is surrounded by three coupled benzoisoindole units to give a 14-π-electron aromatic macrocycle (6). This unique cone-shaped geometry of SubPcs contrasts with the flat or nearly flat structure of most phthalocyanines and provides them with relatively high solubility while lowering their tendency to aggregate.

These characteristics make them attractive as solution-processable photovoltaic materials while their strong absorption in the visible light region, with extinction coefficients of ca. 5×10^4 M^{-1} cm^{-1}, enables them to be used as effective light harvesting components. Indeed, organic photovoltaic cells with PCEs approaching 3% for entirely vapor-deposited systems (7–9) and 1.5% using solution processed thin films of SubPcs as the electron donor and evaporated C_{60} as the electron acceptor (10, 11) have been demonstrated. SubPcs are superior to most phthalocyanines in terms of the open circuit voltage (V_{OC}) obtained in OPVs. The enhancement of the V_{OC} is due to a relative increase in the energy difference (I_G) between the highest occupied molecular orbital (HOMO) of the donor and the lowest unoccupied molecular orbital (LUMO) of the acceptor (12, 13). However, the short-circuit current (J_{SC}) of SubPc-based OPVs is limited because of a narrow absorption spectrum and the amorphous morphology of thin films, which is detrimental to charge transport (12). Therefore, strategies that extend the absorption spectrum and enhance the charge-transport properties of SubPcs films are required to improve their overall device performance.

The molecular structure of SubPcs can be varied via different routes involving peripheral or axial functionalization. Herein, we explore the tuning of the properties of SubPc films through the introduction of axial conjugated ligands that will contribute both to increase light absorption and

* Corresponding author. E-mail: BWMa@lbl.gov (B.M.); frechet@berkeley.edu (J.M.J.F.).
Received for review June 15, 2010 and accepted August 23, 2010
† University of California, Berkeley.
‡ Lawrence Berkeley National Laboratory.
DOI: 10.1021/am100516a

Scheme 1. Preparation of nTp-SubPcs and nTa-SubPcs: (i) 4-Bromophenol, Toluene, 110 °C, 6 h; (ii) Ethyl Magnesium Bromide, 4-Bromophenyl Acetylene, THF, 60 °C, 12 h; (iii) [2,2′-Bithiophen]-5-yl Boronic Acid, Pinacol Ester, $Pd(PPh_3)_2Cl_2$, K_2CO_3, DMF, 80 °C, 5 h; (iv) [2,2′:5′,2″:5″,2‴-Quarterthiophen]-5-yl Boronic Acid, Pinacol Ester, $Pd(PPh_3)_4$, K_2CO_3, DMF, 80 °C, 5 h; (v) Same as iii, but Stirred 3 h; (vi) Same as iv, but Stirred 3 h

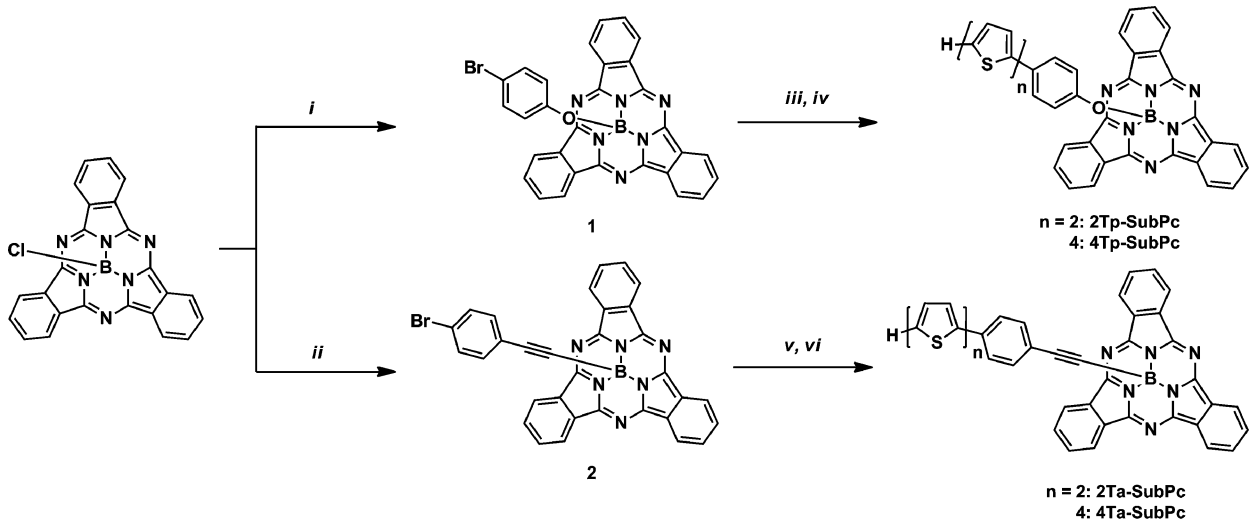

provide a driving force for self-assembly (14). Conjugated ligands featuring bithiophene (2T) and quaterthiophene (4T) moieties were chosen because of the strong $\pi-\pi$ interactions of oligothiophenes that make them crystalline semiconductors able to show high mobility. The synthesis of 2T-SubPcs and 4T-SubPcs is presented, and we show that varying the structure of the SubPc derivatives affects the photophysical, electronic and morphological properties of the materials. Finally, these factors are correlated to the solar cell device parameters.

RESULTS AND DISCUSSION

Rational Design and Synthesis of nT-SubPcs. As shown in Scheme 1, the target axially substituted boron(subphthalocyanine)s (SubPcs) were assembled via Suzuki cross-coupling of thiophene boronic esters and SubPcs bearing an axial phenyl bromide. Phenoxy derivatives were prepared by first treating boron(subphthalocyanine) chloride (Cl-SubPc) with 4-bromophenol in toluene heated at reflux, which yielded **1**. A Suzuki cross-coupling of **1** and either [2,2′-bithiophen]-5-yl boronic acid, pinacol ester or [2,2′:5′,2″:5″,2‴-quarterthiophen]-5-yl boronic acid, pinacol ester yielded, respectively, 2Tp-SubPc and 4Tp-SubPc. Alkynyl derivatives, 2Ta-SubPc and 4Ta-SubPc, were prepared in an analogous fashion from **2**, which was prepared by treating Cl-SubPc with ((4-bromophenyl)ethynyl)magnesium bromide.

The two different linking strategies were chosen because of their effect on the 3-dimensional shape of the resulting molecules. The bent ether bond in the phenoxy SubPcs reduces the symmetry and increases the flexibility of the molecular structure, whereas the alkynyl SubPcs feature a linear carbon−carbon triple bond that leads to more symmetrical and rigid molecules. Conjugated thiophene ligands were introduced to take advantage of the strong $\pi-\pi$ interactions that make oligothiophenes very crystalline and high mobility semiconductors. Crystals of nT-SubPcs were grown and large single crystals of 2Tp-SubPc and 4Tp-SubPc were obtained, which enabled analysis of their crystal structures. The crystal structures reveal the packing mode of these SubPc derivatives, with layers of the conjugated ligands separated by layers of the SubPc macrocycle, as shown in structures a and b in Figure 1. Formation of polycrystalline thin films featuring the same mode of molecular packing would be interesting in an OPV device because the conjugated ligand lamellae could provide high mobility current pathways through the donor layer. In contrast, the crystal structure of the previously studied 2-allylphenoxy-SubPc (7) features slip-stacking of the macrocycles, as seen in Figure 1c. It is clear that the conjugated axial ligands in nT-SubPcs have a significant effect on their molecular packing. Unfortunately, single crystals suitable for structure determination were not obtained for nTa-SubPcs

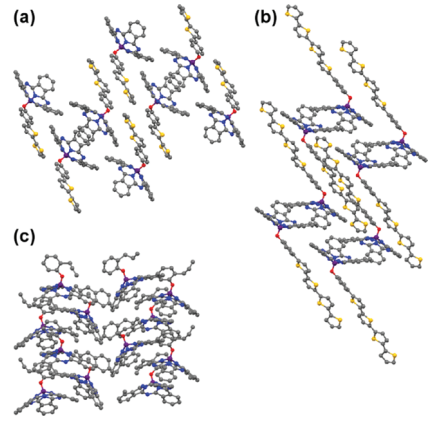

FIGURE 1. View of the crystal packing of (a) 2Tp-SubPc down the *b*-axis, (b) 4Tp-SubPc down the *a*-axis, and (c) 2-allylphenoxy-SubPc down the *c*-axis. Hydrogen atoms have been omitted for clarity, Carbon atoms are represented in gray, nitrogen in blue, boron in purple, oxygen in red and sulfur in yellow. In the crystals, layers of nT-SubPc macrocycles are separated by layers of the conjugated axial ligand, but the macrocycles stack in the absence of a conjugated ligand.

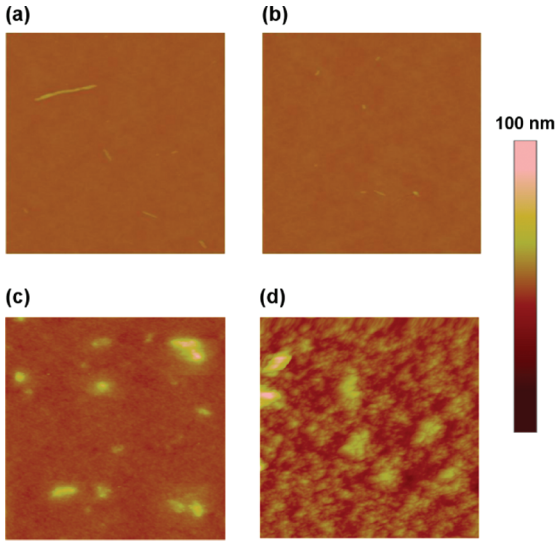

FIGURE 2. 2.0 × 2.0 μm AFM images of (a) 2Tp-SubPc, (b) 2Ta-SubPc, (c) 4Tp-SubPc, (d) 4Ta-SubPc. All films were cast from chlorobenzene.

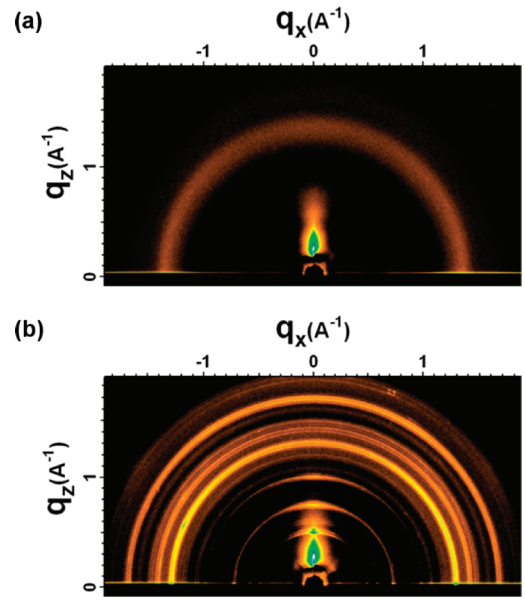

FIGURE 3. GIXS pattern for films of (a) 4Tp-SubPc and (b) 4Ta-SubPc cast from chlorobenzene.

using solvent diffusion techniques because of the reduced solubility of these compounds.

Characterization of Film Morphology. Films of nT-SubPcs were analyzed by AFM and GIXS. AFM was used to measure the roughness of the films, which can be an indication of the crystallinity of the film. Films of 2T-SubPcs (Figure 2a, b) were mostly featureless and very smooth with a root-mean-square (rms) roughness of about 0.5 nm. For films of 4Tp-SubPc (Figure 2c), roughness increased to 1.4 nm, while films of 4Ta-SubPc exhibited the highest roughness of 5.1 nm with a texture clearly visible in Figure 2d. Amorphous films are typically smooth, whereas molecules that tend to aggregate into crystals form relatively rough films. Therefore, these data suggest that 4Ta-SubPc films are more crystalline than films of the other compounds.

To confirm this hypothesis, GIXS patterns of the four compounds were collected. 4Ta-SubPc exhibit many reflections that prove explicitly that the film is polycrystalline, as shown in Figure 3. The signals are stretched into arcs, which indicate that crystalline domains do not have a preferential orientation with respect to the substrate. In contrast, amorphous 2T-SubPcs and 4Tp-SubPc films do not scatter X-rays significantly (see the Supporting Information). The $\pi-\pi$ interactions of the bithiophene ligands do not provide a driving force strong enough to induce crystallization in solution-cast thin films. We believe that the films of 4Tp-SubPc are amorphous because of the lack of symmetry introduced by the bent boron−oxygen−carbon bond linking the ligand to the macrocycle, which inhibits rapid crystallization. Replacement of this ether linkage with an alkyne results in a much more symmetrical molecule in 4Ta-SubPc with a dramatic effect on the crystallinity of the resulting thin films.

OPV Results. Bilayer solar cells were fabricated using solution deposited nT-SubPcs as the donor and evaporated C_{60} as the acceptor. The solar cell results are summarized in Table 1 and representative $J-V$ curves are shown in Figure 4. 2Ta-SubPc and 2Tp-SubPc OPVs were optimized to give the same average PCE of 1.39% with very similar short circuit current (J_{SC}), open circuit voltage (V_{OC}), and fill factor (FF). 4Tp-SubPc solar cells performed relatively poorly with a significantly decreased FF. This decrease in FF is likely due to an increase in the series resistance of the cells. The origin of this effect in this system is not clear, because the space-charge limited mobility of 4Tp-SubPc was found to be the same order of magnitude as that of 2T-SubPcs (1×10^{-6}cm^2/(V s)). However, doping the donor layer in CuPc/C_{60} cells with rubrene has been shown to decrease FF because of charge trapping by rubrene (15). Indeed, 4Tp-SubPc features the highest energy ligand HOMO (see Table 1); thus, ligand charge trapping may play a role in the decreased FF observed. Charge trapping might affect photocurrent measurements more than mobility measurements because mobility measurements are conducted at greater current density than present in OPVs (16).

The small decrease in V_{OC} exhibited by 4Tp-SubPc cells may be explained by its higher lying HOMO level (see Table 1). The lower the energy of the HOMO, the greater is the maximum theoretically attainable V_{OC} value (13). However, 4Ta-SubPc cells possess the lowest V_{OC} of the set, which cannot be explained using this argument because its HOMO level is close to that of 2Tp-SubPc and lower lying than that of 4Tp-SubPc. Furthermore, 4Ta-SubPc cells supplied the highest J_{SC} of the set (−4.48 mA/cm^2), which suggests the morphology of the 4Ta-SubPc film may be affecting these parameters more than the offset of the energy levels. Specifically, crystalline small molecule donors are known to exhibit higher J_{SC} and lower V_{OC} than their amorphous counterparts in bilayer OPVs (17). Therefore, the differences in device characteristics of 4Ta-SubPc solar cells relative to other nT-SubPcs may be explained by the higher crystallinity of the films formed by 4Ta-SubPc. Unfortunately, SCLC measurements could not be performed with 4Ta-SubPc due to inad-

Table 1. SubPc OPV Performance, Electronic, and Photophysical Data

	V_{OC} (V)	J_{SC} (mA/cm^2)	FF	PCE (%)	HOMO[a] (eV)	HOMO[b] (eV)	HOMO-1[b] (eV)	Φ_F
2Tp-SubPc	0.73	−3.72	0.51	1.39	−5.5	−5.06[c]	−5.22[d]	0.02
2Ta-SubPc	0.70	−3.90	0.50	1.39	−5.6	−5.15[d]	−5.18[c]	0.37
4Tp-SubPc	0.63	−3.30	0.34	0.70	−5.3	−4.81[c]	−5.24[d]	0.02
4Ta-SubPc	0.57	−4.05	0.45	1.04	−5.5	−4.89[c]	−5.16[d]	0.35

[a] Average OPV device characteristics for nT-SubPc/C60 bilayer cells. The HOMO levels were estimated from the onset of oxidation relative to ferrocene in dichloromethane. [b] The HOMO and HOMO-1 energies were calculated using DFT. Photoluminescence was measured at room temperature in chloroform solutions, and quantum yields were calculated relative to a cresyl violet perchlorate standard in ethanol, exciting at 546 nm. [c] Orbitals are localized on the ligand. [d] Orbitals are localized on the macrocycle.

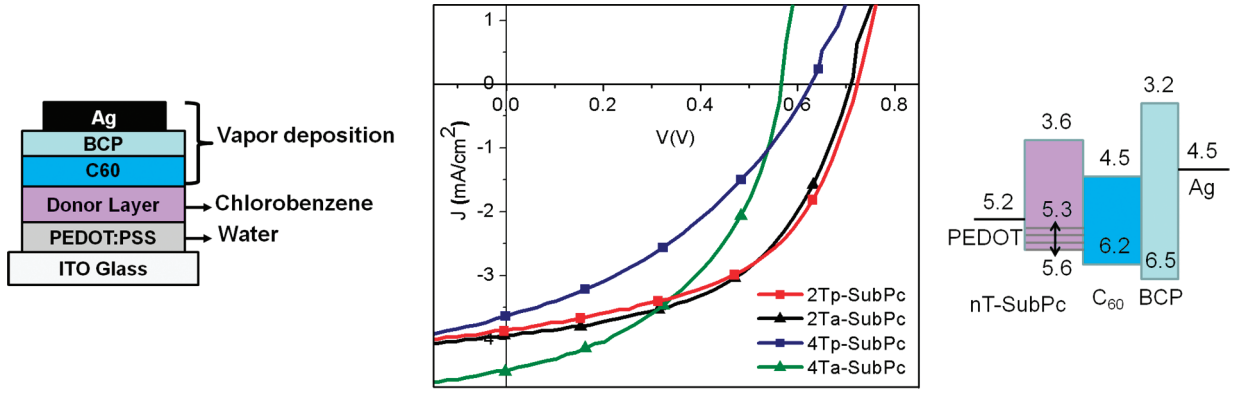

FIGURE 4. Diagrams of a planar heterojunction test structure showing material energy levels and representative $J-V$ curves for nT-SubPc/C_{60} solar cells. PCE(%) for devices shown: 2Tp-SubPc (1.43%), 2Ta-SubPc (1.44%), 4Tp-SubPc (0.85%), 4Ta-SubPc (1.17%).

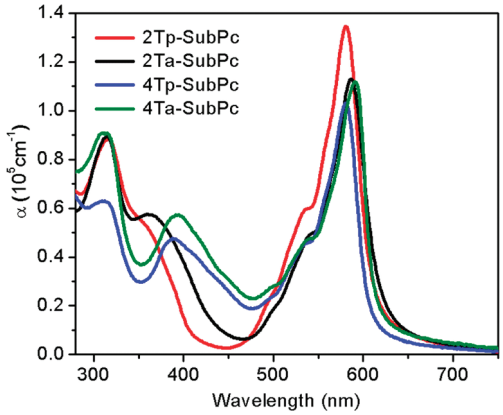

FIGURE 5. UV−visible absorption spectra for nTp-SubPc thin films spun-cast from chlorobenzene.

equate film thickness; therefore, higher charge mobility could not be proven to accompany greater thin film crystallinity.

Electronic and Photophysical Properties. Conjugated ligands give rise to new absorption bands in the UV−visible thin film absorption spectra of nT-SubPcs, which are independent of the SubPc low energy Q-band and high energy Soret band, as shown in Figure 5. Although the absorption of bithiophene ligands overlaps considerably with the Soret band, the absorption of quaterthiophene is still visible in the gap between the two SubPc absorption bands. Small differences in the absorption spectra of the SubPcs may be attributed to the nature of the boron−ligand bond. The intensity of the SubPc Q-band is likely the most important variable because it overlaps well with the solar spectrum and not with the absorption of C_{60}, which becomes significant around 400 nm. The biggest difference in the Q-band is noted between 2Tp and 4Tp-SubPc. In fact, 4Tp-SubPc seems to have the weakest Q-band absorbance of all the nT-SubPcs. The bulky 4T ligand may increase the distance between SubPc macrocycles in thin films and this affects the thin film absorption coefficient of the SubPc chromophore. In contrast to nTp-SubPcs, 2Ta and 4Ta-SubPc exhibit identical Q-band absorbance. The polycrystalline morphology of 4Ta-SubPc likely leads to more optically dense films relative to amorphous 4Tp-SubPc films.

In addition to absorption spectra, the photoluminescence of the nTa-SubPcs and nTp-SubPcs was studied to gain insight into the effects of the conjugated ligands on the excited state of the molecules. Photoluminescence was qualitatively observed only from the SubPc chromophore for all of the nT-SubPcs, which suggests efficient energy transfer from the axial ligands to the SubPc macrocycle. In addition, the nTa-SubPcs are highly fluorescent, but nTp-SubPcs exhibit significant photoluminescence quenching in solution. This phenomenon has previously been observed for SubPcs bearing electron-rich axial ligands that transfer an electron to the excited SubPc (14). Yet, as shown in Table 1, there is no clear correlation between the photoluminescence quantum yield (Φ_F) and the HOMO level of the nT-SubPcs. In addition, Φ_F does not depend on the calculated energy difference between the HOMO and HOMO-1 of nT-SubPcs. This difference is relevant because excitation of the SubPc chromophore leads to a partially filled HOMO-1 in the case of molecules that feature a HOMO localized on the ligand.

The HOMO of each molecule was visualized to determine if it was located spatially on the ligand or the SubPc macrocycle. The electron donating nature of the boryloxy group in nTp-SubPcs clearly destabilizes the ligand electrons relative to nTa-SubPcs. This effect results in the highest energy

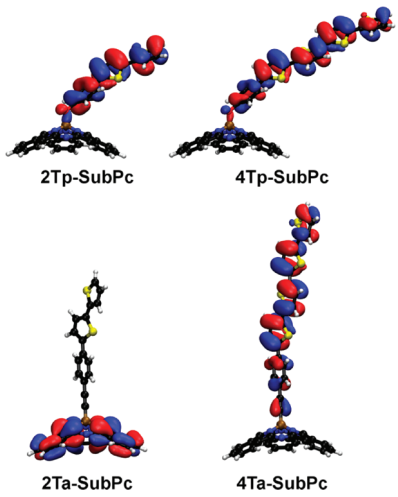

FIGURE 6. Graphical illustrations of the structures of nT-SubPcs overlaid with their respective HOMOs (see the Supporting Information).

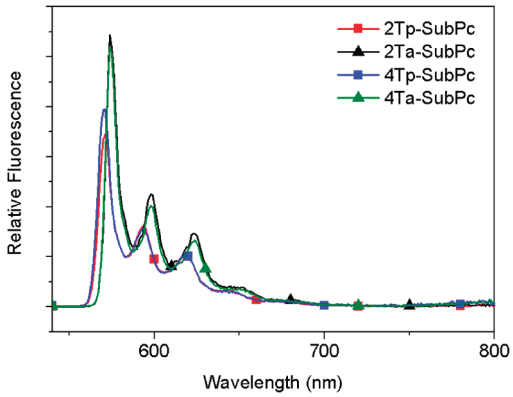

FIGURE 7. Relative fluorescence of nT-SubPcs in 2-methyltetrahydrofuran at 77 K, excited at 530 nm.

electrons residing on the ligand of 2Tp-SubPc and 4Tp-SubPc, as shown in Figure 6. In contrast, the HOMO of 2Ta-SubPc is on the macrocycle, which could explain the high Φ_F of this molecule. Yet, the electron-rich quaterthiophene ligand of 4Ta-SubPc contains the HOMO for that emissive molecule, which suggests that the photoluminescence quenching of nTp-SubPcs is a geometric effect.

Nonradiative relaxation of the excited state of nTa-SubPcs is unfavorable because their overall rigid structure prevents conversion of electronic energy to rotational or vibrational energy. We believe that the bent ether bond in nTp-SubPcs facilitates internal conversion through motion of the axial ligand, a "free rotor" effect. Indeed, freezing the motion of the molecules at 77 K leads to comparable relative fluorescence intensities for each molecule, regardless of the structure, as shown in Figure 7.

The photophysical data presented demonstrate that our conjugated axial ligands contribute to excitation of the SubPc chromophore through energy transfer, but excitation of the SubPc does not necessarily result in charge separation between the thiophene ligand and the relatively electron deficient SubPc unit. However, hole transport in the nT-SubPc films is likely mediated by the relatively easily oxidized conjugated ligands.

CONCLUSIONS

Subphthalocyanine derivatives have been prepared via axial functionalization using phenoxy and alkynyl substitution schemes, and further elaborated with bithiophene and quaterthiophene moieties. The structural differences between these compounds lead to differences in geometry, photophysical properties, electronics, and thin film morphology. nTp-SubPcs are more easily oxidized than analogous nTa-SubPcs, and exhibit efficient photoluminescence quenching through internal conversion. Films cast from solution are only crystalline for the case of 4Ta-SubPc, as shown by AFM and GIXS. This result shows that the tendency of nT-SubPcs to crystallize depends on both the length of the conjugated ligand and the overall symmetry of the molecule.

We have shown that nT-SubPcs perform well in bilayer solar cells with efficiencies over 1 %. The films of 2T-SubPcs are amorphous and therefore provide relatively high values of Voc in solar cells. Formation of crystalline films using 4Ta-SubPc leads to an increase in J_{SC}, but this increase is not enough to improve the PCE of the cell because of a concomitant decrease in V_{OC}. However, this method shows that SubPc macrocycles can be utilized as light harvesting chromophores in a matrix of a crystalline semiconductor that functions as the donor layer in OPVs. Further development of this approach will focus on lower band gap semiconductors that will interact synergistically with SubPc to achieve higher power conversion efficiencies. Theoretical calculations on the charge-separation processes in nT-SubPc/C_{60} heterojunctions are ongoing.

Acknowledgment. This work was supported by the Director, Office of Science, Office of Basic Energy Sciences, Materials Sciences and Engineering Division, of the U.S. Department of Energy, under Contract DE-AC02-05CH11231. Portions of this work (device characterization) were performed at the Molecular Foundry supported by DOE under the same Contract number. Other portions of this work were carried out at the Stanford Synchrotron Radiation Laboratory, a national user facility operated by Stanford University on behalf of he DOE Office of Basic Energy Sciences.

Supporting Information Available: Complete experimental procedures and characterization of 1−2 and 2Tp-SubPc, 4Tp-SubPc, 2Ta-SubPc, and 4Ta-SubPc, and GIXS scattering patterns for nTp-SubPcs and 2Ta-SubPc (PDF); crystallographic data for nTp-SubPcs (CIF). This material is available free of charge via the Internet at http://pubs.acs.org.

REFERENCES AND NOTES

(1) Walker, B.; Tamayo, A. B.; Dang, X.; Zalar, P.; Seo, J. H.; Garcia, A.; Tantiwiwat, M.; Nguyen, T. *Adv. Funct. Mater.* **2009**, *19*, 3063–3069.
(2) Roncali, J. *Acc. Chem. Res.* **2009**, *42*, 1719–1730.
(3) Matsuo, Y.; Sato, Y.; Niinomi, T.; Soga, I.; Tanaka, H.; Nakamura, E. *J. Am. Chem. Soc.* **2009**, *131*, 16048–16050.
(4) Lloyd, M. T.; Anthony, J. E.; Malliaras, G. G. *Mater. Today* **2007**, *10*, 34–41.
(5) Hains, A. W.; Liang, Z.; Woodhouse, M. A.; Gregg, B. A. *Chem. Rev.* 2010, DOI 10.1021/cr9002984.
(6) Claessens, C. G.; Gonzalez-Rodriguez, D.; Torres, T. *Chem. Rev.* **2002**, *102*, 835–854.

(7) Gommans, H.; Cheyns, D.; Aernouts, T.; Girotto, C.; Poortmans, J.; Heremans, P. *Adv. Funct. Mater.* **2007**, *17*, 2653–2658.
(8) Verreet, B.; Schols, S.; Cheyns, D.; Rand, B. P.; Gommans, H.; Aernouts, T.; Heremans, P.; Genoe, J. *J. Mater. Chem.* **2009**, *19*, 5295–5297.
(9) Tong, X.; Lassiter, B. E.; Forrest, S. R. *Org. Electron.* **2010**, *11*, 705–709.
(10) Ma, B.; Miyamoto, Y.; Woo, C. H.; Fréchet, J. M. J.; Zhang, F.; Liu, Y. *Proceedings of Organic Photovoltaics X*; Kafafi, Z. H., Lane, P. A., Eds.; SPIE: Bellingham, WA, 2009; Vol. 7416, p. 74161E.
(11) Ma, B.; Woo, C. H.; Miyamoto, Y.; Fréchet, J. M. J. *Chem. Mater.* **2009**, *21*, 1413–1417.
(12) Mutolo, K. L.; Mayo, E. I.; Rand, B. P.; Forrest, S. R.; Thompson, M. E. *J. Am. Chem. Soc.* **2006**, *128*, 8108–8109.
(13) Rand, B. P.; Burk, D. P.; Forrest, S. R. *Phys. Rev. B* **2007**, *75*, 115327–115338.
(14) Camerel, F.; Ulrich, G.; Retailleau, P.; Ziessel, R. *Angew. Chem., Int. Ed.* **2008**, *47*, 8876–8880.
(15) Chan, M. Y.; Lai, S. L.; Fung, M. K.; Lee, C. S.; Lee, S. T. *Appl. Phys. Lett.* **2007**, *90*, 023504−023506.
(16) Kaake, L. G.; Barbara, P. F.; Zhu, X.-Y. *J. Phys. Chem. Lett.* **2010**, *1*, 628–635.
(17) Perez, M. D.; Borek, C.; Forrest, S. R.; Thompson, M. E. *J. Am. Chem. Soc.* **2009**, *131*, 9281–9286.

AM100516A